# Photoelectrochemical imaging system for the mapping of cell surface charges

Fan Wu[1,2], Bo Zhou[1], Jian Wang[2], Muchun Zhong[1], Anirban Das[1], Michael Watkinson[3], Karin Hing[1], De-Wen Zhang[2*], Steffi Krause[1*]

[1]School of Engineering and Materials Science, Queen Mary University of London, Mile End Road, London E1 4NS, UK

[2]Institute of Medical Engineering, School of Basic Medical Sciences, Xi'an Jiaotong University Health Science Center, Xi'an, 710061, China

[3]The Lennard-Jones Laboratories, School of Chemical and Physical Sciences, Keele University, Staffordshire, ST5 5BG, UK

s.krause@qmul.ac.uk, zhangdewen@xjtu.edu.cn

## ABSTRACT

The surface charge of cells affects cell signaling, cell metabolic processes, adherence to surfaces and cell proliferation. Our understanding of the role of membrane charges is limited due to the inability to observe changes without interfering, chemically or physically, with the cell or its membrane. Here, we report that a photoelectrochemical imaging system (PEIS) based on label-free ac-photocurrent measurements at indium tin oxide (ITO) coated glass substrates can be used to map the basal surface charge of single live cells under physiological conditions. Cells were cultured on the ITO substrate. Photocurrent images were generated by scanning a focused, modulated laser

beam across the back of the ITO coated glass substrate under an applied bias voltage. The photocurrent was shown to be sensitive to the negative surface charge of the substrate facing, basal side of a single living cell – an area not accessible to other electrochemical or electrophysiological imaging techniques. The PEIS was used to monitor the lysis of mesenchymal stem cells.

There is a major drive to develop methodologies for monitoring cellular processes in order to improve our understanding of physiological events such as cell signaling, attachment and development and to investigate the response of cells to surfaces and drugs at an ultrastructural and microscopic level as this could aid the development of tissue regenerative materials and disease combating drug design. The surface charge of cells is thought to affect inter-cell communication[1-3], their adherence to surfaces[4-6], their uptake and release of molecules[7] and their development and division[8, 9]. There is also a close link between surface charge and membrane potential[10]. However, our understanding of the role of surface charge is limited due to the lack of experimental tools to observe changes in surface charge in response to factors associated with health or disease with good spatial resolution without chemically or physically interfering with the cell or its membrane. Methods for measuring cell charges and membrane potentials include zeta potential measurements and electrophoresis[11], which can only measure the charge of whole cells, and potential sensitive dyes[12] and charged nanoprobes[13] that can adversely interfere with the biology of cells.

Label-free electrochemical imaging techniques provide a good alternative to standard electrophysiological measurements. Plasmonic-based electrochemical impedance microscopy (P-EIM) has been used for imaging cell impedance[14] and action potentials[15]. Scanning electrochemical microscopy (SECM) has been applied extensively to studying cell activity and metabolism with high spatial resolution[16, 17]. Scanning ion conductance microscopy (SICM) is a powerful tool for imaging of cell

topology and has recently been used to image cell-surface charges[18, 19]. Like all scanning probe techniques, SICM provides high spatial resolution, but only allows relatively slow imaging of the apical side of cells. To date, no charge mapping of the surface facing, basal side of cells, which is of particular interest for tissue engineering applications such as the design of scaffolds, has been carried out.

Light-addressable potentiometric sensors (LAPS) are based on photocurrent measurements at electrolyte-insulator-semiconductor (EIS) field-effect structures under an applied bias and can be used to map the surface potential of the insulator by scanning the semiconductor with a focused, modulated laser beam without the need for a scanning probe[20]. In contrast to scanning probe techniques such as SICM, LAPS imaging can be carried out with high speed using a mirror scanning setup[21] or by simultaneous multipoint measurements[22]. LAPS are sensitive to charge and have been able to visualize cell surface charges of multilayer yeast cells, but only when there is a direct contact between insulator and cell[23]. In normal viable cell culture, the gap between the insulator surface and the cell membrane (> 10 nm)[24, 25] and the short Debye length (< 1 nm) under physiological conditions with high ionic strength (~150 mM)[18] prevents any response of LAPS to the cell surface charge.

Recently, electrolyte-semiconductor (ES) structures without an insulator have been shown to be suitable for ac-photocurrent imaging with a good spatial resolution of 2 µm[26]. The ac-photocurrents at these structures feature redox currents, resulting in a photoelectrochemical imaging system (PEIS), which combines the advantages of

LAPS imaging by employing a high-resolution LAPS setup developed previously[27, 28] and recently reported light-addressable electrodes (also named light-activated electrochemistry) (LAE)[29-37]. LAE have been developed based on different semiconductor materials including monolayers of CdS quantum dots[33] or carbon dots[38], $TiO_2$[29, 31], ZnO nanorods[39], InGaN/GaN nanowires[34], indium tin oxide (ITO)[26], amorphous silicon[32], α-$Fe_2O_3$[30] and silicon protected with self-assembled organic monolayers[40, 41]. While the organic monolayer limits the potential range silicon can be used in, metal oxide semiconductors such as ITO have the advantage that they can be used at anodic potentials without suffering significant damage, thereby obviating the need for a redox mediator, which could potentially interfere with the cell biology when used for cell imaging applications.

Herein, we use ac-photocurrent imaging at ITO coated glass substrates for mapping of cell surface charges of the basal, substrate facing side of various viable mammalian cells both in buffered electrolyte solution and cell culture medium, for the first time.

## EXPERIMENTAL SECTION

**Materials.** ITO coated glass (50 Ω/sq, ~140 nm ITO on 0.5 mm thick glass) was purchased from Diamond Coatings Limited, UK. Human Mesenchymal Stem Cells (hMSC), Mesenchymal Stem Cell Growth Medium 2 (Cat No. C-28009) and the SupplementMix (Cat No. C39809) were purchased from PromoCell. All other chemicals were purchased from Sigma-Aldrich, including the cell culture materials of Dulbecco's Modified Eagle's Medium (DMEM, Cat No D6429), Fetal Bovine Serum

(FBS, Cat No F9665), penicillin-streptomycin (Cat No P4333), Dulbecco's Phosphate Buffered Saline (DPBS, pH 7.4, 10 mM phosphate buffer solution containing 137 mM NaCl and 2.7 mM KCl) and Trypsin-EDTA (Cat No T3924). All solutions were prepared using ultrapure water (18.2 MΩ·cm) from a Milli-Q water purification system (Millipore, USA). MG63 Human osteosarcoma cells (Cat No 86051601) and B50 rat neuroblastoma cells (Cat No 85042302) were purchased from Sigma-Aldrich.

**Preparation of ITO Coated Glass.** The ITO coated glass was cut into 1 cm × 1 cm pieces. They were cleaned by ultrasonication for 15 min with acetone, isopropanol, and ultrapure water. After drying with nitrogen, the ITO coated glass was kept at room temperature before use.

**Cell Culture on ITO Coated Glass Substrates.** Before seeding cells, ITO coated glass substrates and PEIS chamber were sterilized with 70% ethanol and rinsed thoroughly with sterilized water and sterilized DPBS solution and blown dry. MG63 human osteosarcoma cells and B50 rat neuroblastoma cells were cultured in a T75 cell culture flask with DMEM supplemented with 10% FBS and 1% penicillin-streptomycin solution, while hMSCs were cultured in a medium containing Mesenchymal Stem Cell Growth Medium 2 supplemented with 10% SupplementMix and 1% penicillin-streptomycin in a humidified atmosphere with 5% $CO_2$ at 37°C with the medium changed every two days. At confluence, cells were trypsinized and resuspended in 10% FBS supplemented DMEM for seeding. For single cell imaging with PEIS, cells were seeded onto the ITO coated glass surface in the assembled PEIS

chamber at a concentration of $2.5x10^4$ cells/mL and incubated at 37 °C with 5% $CO_2$ for 24 hours. For PEIS measurements, both DPBS solution and 10% FBS supplemented DMEM were used as the electrolyte. To obtain confluent layers of cells on the ITO coated glass substrates used for impedance spectroscopy and chronoamperometry, cells were seeded at a higher concentration of $1.5x10^5$ cells/mL and incubated at 37 °C with 5% $CO_2$ for 48 hours.

The effect of PEIS imaging on cell viability was investigated using a fluorescence live/dead assay (Thermo Fisher Scientific, cat. no.: L3224). MG-63 cells were seeded onto two pieces of ITO coated glass assembled in the PEIS chamber at a concentration of $6.7x10^5$ cells/mL and incubated at 37 °C with 5% $CO_2$ for 24 hours. One ITO chip was subjected to a PEIS raster scan in DPBS while another stayed under ambient conditions for the same time. Then, 0.5 mL of 2 μM calcein AM, 4 μM ethidium homodimer-1 and 8.12 μM of Hoechst 33342 was used to test the viability of the cells with and without PEIS imaging. Three different areas in each sample were checked using a fluorescence microscope (Leica DMI4000B Epifluorescence, see sample images in Figure S1), and resultant images were processed with Image J software for counting cells.

To induce cell lysis, 0.04% v/v Triton X-100 (TX-100) in DPBS was added as electrolyte after one PEIS photocurrent image of hMSC was obtained, followed by several continuous PEIS raster scans to monitor the whole process.

**Zeta Potential Measurements of Cells**

For three types of cells, cell suspensions in DPBS buffer were kept at a concentration of $1.35x10^5$ cells/mL. The measurements were performed in disposable folded capillary zeta cells with gold-plated electrodes at 25 ℃ using the electrophoretic light scattering technique on a Zetasizer Nano ZS analyzer (Malvern Instruments, GB), and measurements for each type of cell were conducted 5 times.

**Chronoamperometry and Impedance Measurements.** Chronoamperometry and impedance measurements were carried out in the DPBS solution using an Autolab PGSTAT30/FRA2 (Windsor Scientific Ltd, UK) using a platinum electrode and an Ag/AgCl electrode as the counter and reference electrodes, respectively. A diode laser ($\lambda$ = 405 nm, max 500 mW), which was chopped at 10 Hz, illuminated the ITO substrate when recording the current-time (*I-t*) curves.

**PEIS Measurement.** The PEIS setup is shown in Figure S2. A laser diode module LD1539 (Laser 2000, $\lambda$=405 nm, max. 50 mW) was used for charge carriers generation. The laser intensity was sinusoidally modulated at 10 Hz for all PEIS measurements. The beam profile of the laser diode module was improved by using a spatial filter and a collimator lens. The laser was focused onto the ITO coated glass substrate using an LD Plan-NEOFLUAR 40× objective with a correction ring (Zeiss, numerical aperture 0.6), which allowed to correct for spherical aberration caused by focusing through a solid substrate. The sample holder was mounted onto an M-VP-25XL XYZ positioning system with a 50 nm motion sensitivity on all axes (Newport, UK). A white light illuminated the sensor from the front side to obtain an

optical image of the sensor surface with the CMOS camera. The photocurrent was measured using an EG&G 7260 lock-in amplifier. The control program used for the measurements was written in LabView[27].

## RESULTS

The electrochemical behavior of ITO in Dulbecco's phosphate buffered saline (DPBS) was investigated with the experimental setup shown in Figure S2.

### Electrochemical Properties of the Electrolyte-Semiconductor Interface

Figure 1a shows the capacitance-voltage curve of the ITO electrode in DPBS solution in the dark, which was obtained by measuring impedance spectra (Figure S3) at a series of dc voltages from -0.1 V to 1.5 V with a step of 0.2 V and then fitting these spectra with an equivalent circuit consisting of a serial combination of the solution resistance (R) and a constant phase element (CPE) to obtain the capacitance values at each voltage (Table S1). The capacitance decreases with increasing voltage. At 1.5 V, the capacitance is 2.8 $\mu F/cm^2$, which is much smaller than the double layer capacitance (~10 $\mu F/cm^2$), confirming the formation of a depletion layer in the ITO at the interface to the DPBS solution as expected for an n-type semiconductor.

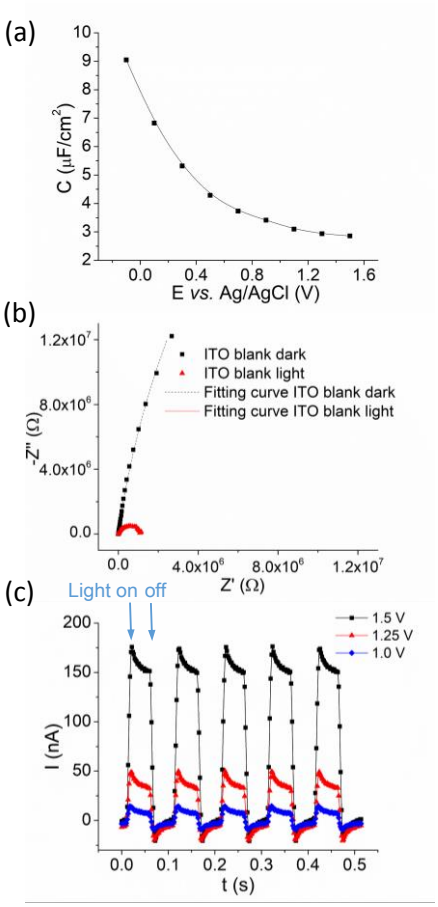


*Figure 1. Electrochemical properties of the ITO in DPBS. (a) Capacitance-voltage curves; (b) Nyquist plots (dots) and corresponding equivalent circuit fits (lines) of ITO in PBS at a bias voltage of 1.5 V vs. Ag/AgCl in the dark (black) and with blue laser illumination of the entire surface (red); (c) I-t curves recorded at different bias voltages (1.5 V, 1.25 V and 1.0 V) with blue laser illumination chopped at 10 Hz.*

To investigate the effects of light on the interfacial properties of the ES structure, electrochemical impedance spectra were recorded at 1.5 V both in the dark and under constant illumination of the entire sample (Figure 1b). The corresponding Bode plots are presented in Figure S3. A significant impedance decrease was observed under illumination at frequencies below 10 Hz. Turning on the laser illumination caused the appearance of a charge transfer resistance of 1.12 MΩ indicating a light-induced charge transfer process at the interface of the ITO electrode and DPBS solution at 1.5

V, which was attributed to the oxidation of hydroxide ions.

Chronoamperometry with chopped blue laser illumination at 10 Hz at different applied voltages was performed to obtain the time dependence of the current signal (Figure 1c). When the light was turned on, an increase in the current was observed for the first 20 ms followed by a drop in the current over a period of about 28 ms to a constant value. At 1.5 V, the current drop, which can be attributed to surface recombination of charge carriers[42], was about 14% of the overall current. Turning off the light caused the current to drop to its minimum value within 12 ms.

**PEIS Imaging of the Surface Charge of a Polycation**

To verify the ability of using ITO based PEIS to image the surface charge, a dot of the polycation polyallylamine hydrochloride (PAH) was drop coated from a 20% (w/w) aqueous solution onto the ITO coated glass surface and allowed to dry. A polycation was chosen rather than a polyanion, as the positive charge was expected to cause an increase in the local photocurrent, thereby avoiding a convolution of charge and impedance effects that would be expected for a negatively charged polymer. Figure 2a shows the PEIS image of the PAH dot coated ITO surface with a focused laser beam modulated at a frequency of 10 Hz at a bias voltage of 1.5 V. The resolution of photocurrent imaging with ITO coated glass under these conditions was previously determined to be 2.3 μm[26]. At the selected voltage, the photocurrent on the PAH dot was greater than that of the blank ITO surface as illustrated in the PEIS image (Figure 2a) and the corresponding *I-V* curves measured on the PAH dot and on the blank ITO

surface (Figure 2b), respectively. This is due to the positive surface charge introduced by the PAH, which increases the local concentration of negatively charged ions including that of hydroxide ions and therefore enhances the anodic oxidation process on the electrode surface. To verify this, chronoamperometry with chopped laser illumination at 10 Hz was performed on the same PAH dot patterned sample at a bias voltage of 1.5 V on the PAH dot coated area and the blank ITO surface (Figure 2c). The initial increase in the current was greater on the PAH coated area than that measured on the blank ITO surface, while the transient current drop was not significantly affected by the PAH. Electrochemical impedance measurements were also carried out on the same PAH dot coated ITO sample with the laser illuminating the PAH coated area with a light spot of 500 μm diameter or the blank ITO surface with a light spot of the same size, respectively. Figure S4 shows the corresponding Nyquist plots, revealing a smaller charge transfer resistance on the PAH coated area compared to the blank ITO surface under illumination and at a bias voltage of 1.5 V, which verified an enhanced anodic oxidation process induced by the positive surface charge of PAH. Thus, PEIS was successfully applied to the imaging of surface charges.

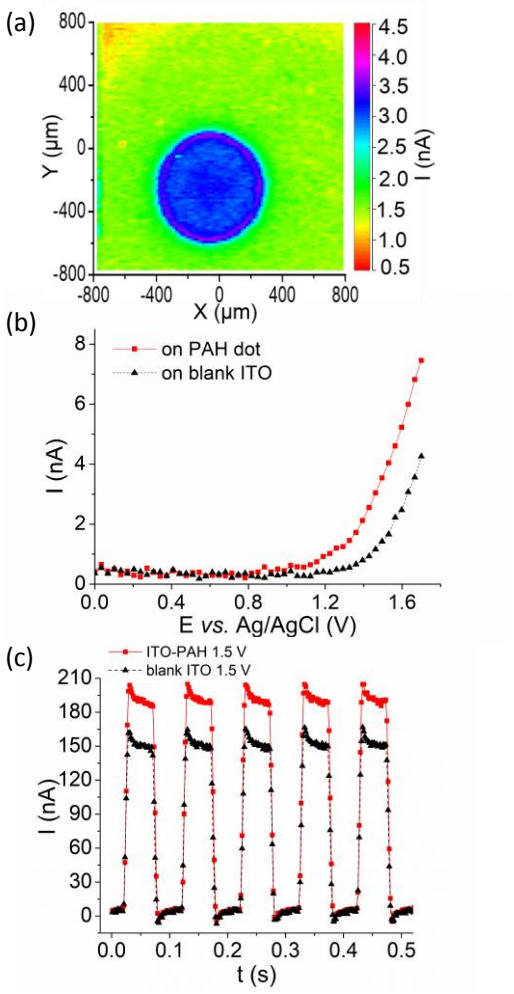


*Figure 2. (a) PEIS image of a PAH dot patterned ITO coated glass surface at 1.5 V and a frequency of 10 Hz and (b) corresponding I-V curves on the PAH dot (red) and on the blank ITO surface (black) (c) I-t curves recorded at 1.5 V with modulated blue laser illumination of 10 Hz on a PAH covered ITO sample (red) and a blank ITO surface (black).*

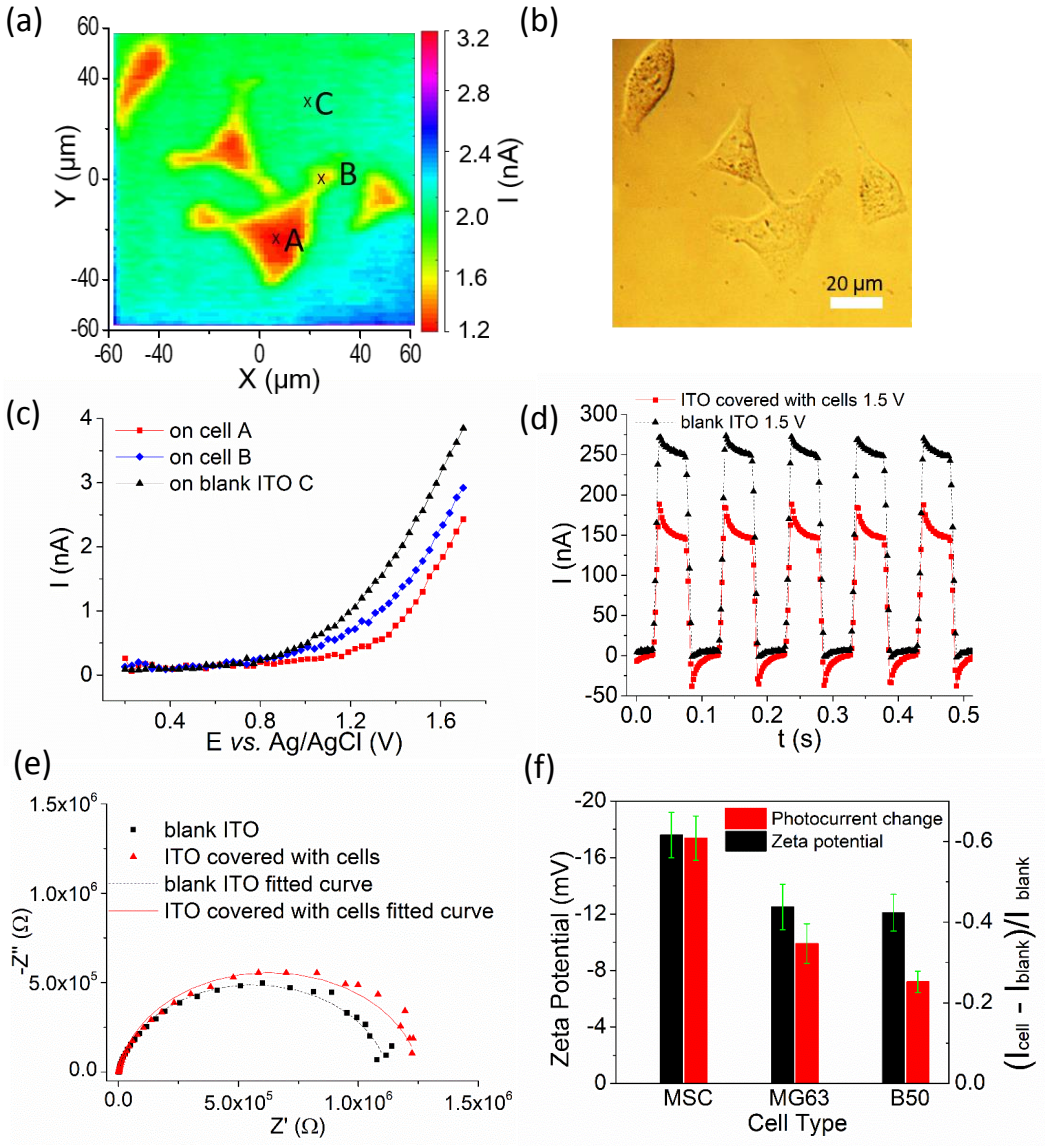


*Figure 3. Photocurrent imaging of single cells (a) PEIS image of four MG63 human osteosarcoma cells on an ITO coated glass surface at 1.5V and a frequency of 10 Hz and corresponding (b) optical image and (c) I-V curves on cell (point A red and B blue) and off cell C (black) (measurement spots are marked with x); (d) I-t curves recorded at 1.5 V with chopped blue laser illumination of 10 Hz on cell covered ITO sample (red) and blank ITO surface (black); (e) Nyquist plots (dot) and corresponding equivalent circuit fits (lines) of ITO electrode covered with cells (red) and blank ITO electrode (black) at 1.5 V under a constant blue laser illumination, respectively; (f) Comparison of zeta potentials and photocurrent contrasts for three different cell types. The photocurrent contrast for individual cells was determined from the average photocurrent of line scans through the main body of the cells. The error bars represent the standard deviations calculated from 5 repeat measurements for the zeta potential and 4 repeat measurements with different cells for the photocurrent contrast.*

**PEIS Imaging of Single Cells**

Figure 3a shows the PEIS image of four MG63 human osteosarcoma cells on ITO coated glass at 1.5 V measured with a light modulation frequency of 10 Hz, which shows good correlation with the optical image obtained from the camera (Figure 3b). The photocurrent on the cells was smaller than that on the bare ITO surface, which, in keeping with the PAH model study (see above), we assume to be due to the negative charge of the cell surface. Chronoamperometry with chopped blue laser illumination at 10 Hz on ITO samples with and without a confluent layer of cells shows a significantly smaller current increase upon illumination for the sensor with cells than for the one without (Figure 3d). Figure 3e shows the Nyquist plots of the ITO electrode with and without cells in PBS at 1.5 V under illumination, where a greater charge transfer resistance was obtained on the cell-covered ITO electrode compared to the blank ITO electrode, indicating a blocked redox process caused by the negative surface charge of the cells on the ITO electrode surface. The frequency dependence of the local photocurrent (Figure S5) shows the greatest contrast between blank surface and cell attachment area at low frequencies. This also confirms that the ac-photocurrent contrast is caused by the redox process as the time-dependent photocurrent (Figure 3d) reaches a constant steady state oxidation current after about 58 ms, i.e. at high frequencies, the redox current would not reach its maximum value. It is also worth noting that the PEIS image of cells shown in Figure 3a presents a photocurrent distribution along the cells, where the photocurrent in the cell center was

smaller than the photocurrent on the cell edge, which can also be seen from the *I-V* curves displayed in Figure 3c measured at different points on a cell (points A and B) and off the cell (point C). These local differences in the photocurrent under the cell could be due to differences in the local cell surface charge or the gap height between the surface and the cell membrane as the cell can also physically block the diffusion of hydroxide to the sensor surface. The diffusion path in the narrow gap under the cell is longer in the center of the cell resulting in lower photocurrents. To confirm that the photocurrents under the cell are dependent on the cell surface charge, the results for three different cell types were compared with their zeta potentials. Figures S6 and 4a show ac-photocurrent images of B50 rat neuroblastoma and human mesenchymal stem cells (hMSC), respectively. The three cell types display significant differences in the photocurrent contrast, which show a clear correlation with cell charges determined by zeta potential measurements (Figure 3f).

Besides imaging single cells in DPBS solution with PEIS, the surface charge of single cells was also visualized successfully in Dulbecco's Modified Eagle's Medium (DMEM) supplemented with 10% FBS (Figures S7 and S8), which makes PEIS a suitable technique for use under standard mammalian cell culture conditions.

For all photocurrent images of cells presented in this work, optical images taken before and after photocurrent imaging showed that the cells were not adversely affected by the laser light, the applied voltage and the photocurrent. Cell viability measurement of MG-63 cells after a photocurrent raster scan showed that 97.01% ±

0.21% of the cells on the surface were viable compared to 97.24% ± 0.08% on a control sample (Figure S1). It is assumed that this is due to the relatively small photocurrents (< 4 nA) and the fact that the potential drop will occur across the space charge layer and the double layer, which are not in immediate contact with the cell membrane. To exclude any potential damage due to the laser light, a shorter wavelength laser, which is completely absorbed by the ITO, could be employed in the future.

**Monitoring Cell Lysis with PEIS**

The cell surface charge is derived from phospholipids head groups in its membrane. To validate PEIS further, dynamic changes of cell membrane triggered by introduction of a nonionic surfactant were monitored by photocurrent imaging. TX-100 is a commonly used nonionic surfactant for membrane permeabilization and lysing cells by means of disrupting the lipid bilayer, solubilizing membrane-bound proteins, and ultimately destroying the compactness and integrity of the lipid membrane[43, 44].

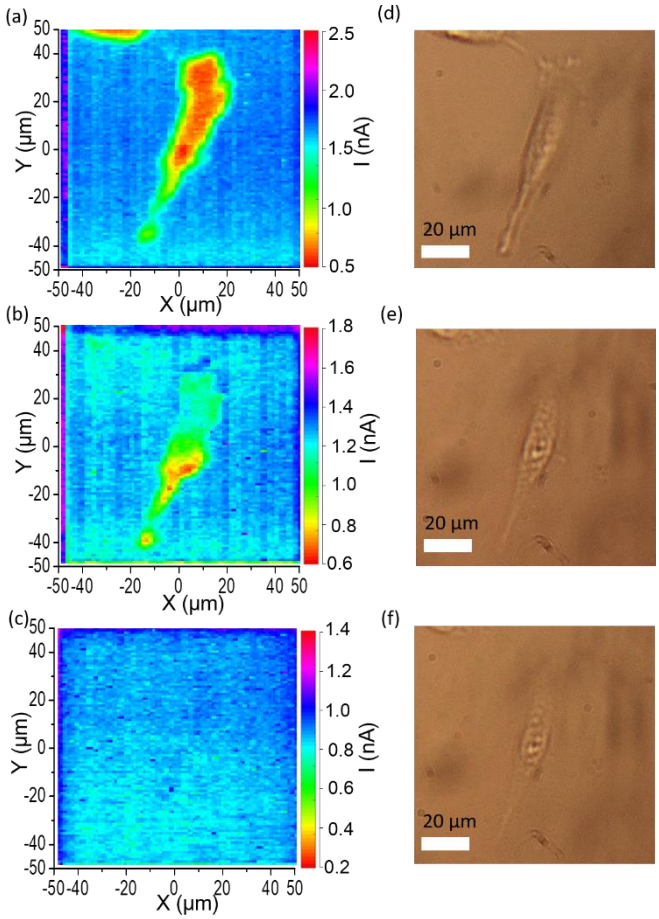


*Figure 4. Photocurrent and optical imaging before during and after cell lysis (a) PEIS image of a hMSC before lysis in DPBS (b) PEIS image after 30 min incubation with 0.04% TX-100 in DPBS (c) PEIS image after 200 min incubation with 0.04% TX-100 in DPBS; (d), (e) and (f) are the corresponding optical images.*

The process of cell lysis was triggered by incubation in 0.04% v/v TX-100 (0.68 mM) in DPBS and recorded by PEIS. In the absence of TX-100, the PEIS image (Figure 4a) shows a clear photocurrent distribution of the cell and an intact cell membrane profile in accordance with the corresponding optical image (Figure 4d). 30 min after adding TX-100, the PEIS image (Figure 4b) and optical image (Figure 4e) show that the cell lost its integrity and the photocurrent within the cell increased indicating progressive solubilization of the lipid membrane and a progressive leakage of electrolyte through

the cell membrane. 200 min after adding TX-100, the cell profile in the LAES image disappeared indicating a complete breakdown of membrane, which is matching the optical image (Figure 4f) where only a residue of the cell remained. Normalized photocurrent lines scans through the center of the cell (at $X$=0 in the images in Figures 4a-c) demonstrate the increase in the photocurrent during cell lysis (Figure S9). In contrast, a lower concentration of 0.01% TX-100 (0.17 mM) failed to solubilize the cell membrane during 200 min observation. These results are in accordance with an investigation of the effect of TX-100 on the permeability of cell membranes with SECM[45] and the effect of TX-100 concentration on lipid bilayers by AFM[46].

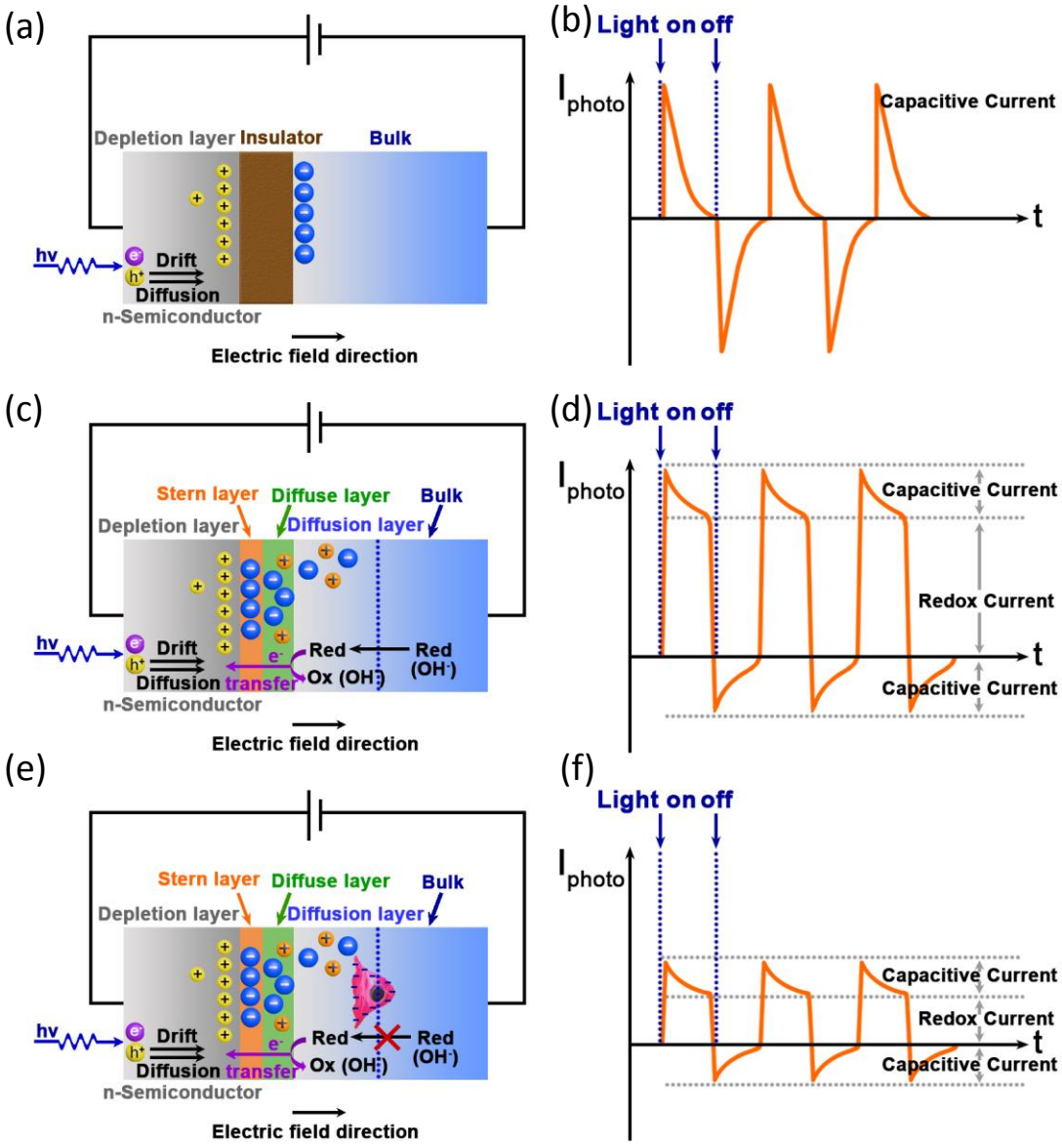


*Figure 5. Schematic of the principle and transient photocurrents of LAPS and PEIS. (a) Traditional LAPS system with an Electrolyte-Insulator-Semiconductor (EIS) structure and (b) the corresponding photocurrent signal vs. time under chopped light illumination; (c) PEIS system with an Electrolyte-Semiconductor (ES) structure and (d) the corresponding photocurrent signal vs. time under chopped light illumination; (e) PEIS system used for single cells measurement and (f) the corresponding photocurrent signal vs. time under chopped light illumination.*

## DISCUSSION

The main question posed by the results presented here is: Why is PEIS sensitive to negative cell surface charges in viable cell culture, while LAPS is not? The main difference in the two techniques, as has already been hinted at, is the presence of a redox current in PEIS. The basic concept for the current signal generation in PEIS is illustrated in Figure 5. Compared to the traditional LAPS system with an EIS structure (Figure 5a), ITO based PEIS is based on an ES structure (Figure 5c). Figures 5b and d show schematic representations of the current signals from EIS and ES structures illuminated with chopped light with an applied bias voltage. In the LAPS system, when the light is switched on, the generated charge carriers separate in the space charge region, resulting in a transient current spike, which charges the capacitive structure. While the light intensity stays constant, the current in the outside circuit decreases to zero because of the existence of the insulator. When the light is switched off, the capacitor is discharged, resulting in a reverse transient current spike and the current declines to zero as the light stays off.

In the PEIS system, when the light is on, the light-induced charge carriers do not only separate in the space charge region but also transfer through the semiconductor-electrolyte interface, causing an additional redox current to flow in the outer circuit. Thus, the photocurrent spike detected in PEIS consists of two parts, the depletion layer charging current and the redox current (Figure 5d). When the light

intensity remains constant, the current does not decrease to zero, but to the value of the redox current since the redox process continues. When the light is switched off, the redox process is inhibited and the current signal decreases to the background dark current showing a negative current spike due to the depletion layer discharging process. Figure S10a shows the band model of the ITO semiconductor-electrolyte interface under illumination with an applied anodic potential. The bands are bent upwards, which forms a growing barrier for interfacial electron transfer from the bulk of the semiconductor to the interface. Figure S10b shows the positions of different standard electrode potentials. Due to a high overpotential of the ITO surface, the oxygen production from the oxidation of hydroxide at an anodic potential of 1.5 V (vs. Ag/AgCl reference electrode) is not obvious. Hence, the light-induced anodic process is more likely to be the oxidation of $OH^-$ to hydroxyl radicals ($OH^{\cdot}$) (demonstrated at $TiO_2$ by Jaeger and Bard[47]).

Surface charge imaging with the ITO based PEIS was verified using a PAH dot patterned ITO surface. The positive surface potential introduced by the PAH increased the local potential and enhanced the anodic process on the electrode surface resulting in a greater photocurrent on the PAH dot compared to the blank ITO surface in PEIS measurements. In contrast, the photocurrent detected under living cells was smaller than that on the blank ITO surface. This raised the question whether the reduction in photocurrent was caused by the negative cell surface charge or only by the diffusion of hydroxide through the narrow gap between the cell and the ITO surface. The

measurement problem is analogous to that encountered in SECM with nano-gaps. Tan et al.[48] have recently shown that charge has a profound effect on diffusion limited SECM currents measured across gaps of tens of nm even with high supporting electrolyte concentrations. Their model takes into account changes of local ion concentrations due to the surface charge, which in turn affects the diffusion of charged species to the electrode surface. Figures 5e and f illustrate the current signal change when live cells are cultured on the ITO substrate. The negative surface charge of the cells repels the hydroxide ions in the electrical double layer, effectively lowering the amount of hydroxide arriving at the ITO surface by diffusion resulting in a smaller redox current compared to the blank electrode surface. This explains why we cannot only see charge effects within the Debye length of the semiconductor surface, but the sensitivity of PEIS also extends to charges in the diffusion layer. The model and experimental results presented by Tan et al.[48] together with the fact that we have found a strong correlation between the zeta potential and the photocurrent contrast for different cell types shows that the photocurrent images at ITO coated glass are significantly affected by the surface charge of cells. Quantitative modelling of the surface charge of cells would require treating PEIS as an inverted SECM, where the electrode can be regarded as a disk electrode of the size of the illuminated area with the dark area as an infinitely thick insulating sheath and the cell as an insulating substrate as the flux from hydroxide ions comes from the solution and not from the cell. The current at an electrode in close proximity to an insulating substrate is

determined by the diffusion of reactants into the gap between electrode and substrate and depends strongly on the distance between them [49]. In the case of PEIS at living cells, the gap between cell membrane and ITO surface is unknown, although methods for the measurement of the gap height have been described, which may be employed for quantitative modelling in the future [24, 25, 50]. An added complication is the irregular shape of cells, which also affects the diffusion profile. We are planning to calibrate surface charge measurements by placing an electrode of known charge at defined distances from the ITO surface in the future. It is, however, likely that PEIS will be more useful in monitoring relative changes in cell surface charge rather than measuring absolute charge.

## CONCLUSIONS

This work has demonstrated a novel photoelectrochemical imaging system (PEIS) based on ac-photocurrent measurements at ITO coated glass substrates for imaging the surface charge of single live cells under physiologically relevant conditions, including the presence of serum proteins. The technique images the basal, substrate facing side of the cell, which is not accessible to other electrochemical or electrophysiological imaging techniques. This makes it a useful tool for the investigation of cell responses in cell culture. We have demonstrated that PEIS can be used to monitor cell lysis. In the future, PEIS can be applied to the investigation of the metabolic processes of single cells, the differentiation or proliferation of cells on different types of surfaces to aid the development of tissue engineering materials and

for high-throughput screening of drug induced cell responses and as a diagnostic tool to distinguish healthy and diseased cells. As demonstrated with the model system of a charged polymer, PEIS is also more broadly applicable to charge measurements at materials interfaces.

**ACKNOWLEDGEMENTS**

The authors are grateful to the China Scholarship Council for providing a PhD studentship to FW, BZ and MZ, to the EU for providing Marie Skłodowska-Curie Individual Fellowships to DZ and AD (H2020-MSCA-IF-2014-660489, H2020-MSCA-IF-2016-745820) and to BBSRC (BB/P026788/1) and EPSRC (EP/R035571/1) for funding.

**AUTHOR CONTRIBUTIONS**

F.W. and B.Z. contributed equally to this paper. F.W. did photocurrent imaging with PAH, human osteosarcoma and rat neuroblastoma cells and electrochemically characterised ITO in DPBS. B.Z. did photocurrent imaging with human mesenchymal stem cells (hMSC), investigated the lysis of hMSCs and did zeta potential measurements with all three different cell types. J.W. and M.Z. developed cell culture conditions and recorded PEIS and LAPS images with cells. A.D. contributed to the interpretation of the photocurrent data. K.H. provided guidance for the cell culture and co-wrote the paper. S.K., D.-W.Z. and M.W. designed the experimental program, coordinated the project and co-wrote the paper.

**ASSOCIATED CONTENT**

Supporting information accompanies this paper:

- Cell viability experiment
- Schematic of experimental setup
- Impedance spectra of ITO in DPBS
- A table of equivalent circuit fit results for the above impedance spectra
- Frequency dependence of the local photocurrent
- Impedance spectra of ITO with and without PAH coating under illumination
- PEIS image of B50 cells in DPBS
- PEIS images of MG63 and B50 cells in cell culture medium
- Normalized photocurrent lines scans through an hMSC before and after addition of TX-100
- Energy level diagrams in the ITO-electrolyte system

## REFERENCES


1. Christianson, H. C.; Svensson, K. J.; van Kuppevelt, T. H.; Li, J. P.; Belting, M., Cancer cell exosomes depend on cell-surface heparan sulfate proteoglycans for their internalization and functional activity. *Proc. Natl. Acad. Sci. U. S. A.* **2013,** *110* (43), 17380-17385.
2. Lee, K. D.; Hong, K.; Papahadjopoulos, D., Recognition of liposomes by cells - invitro binding and endocytosis mediated by specific lipid headgroups and surface-charge density. *Biochimica Et Biophysica Acta* **1992,** *1103* (2), 185-197.
3. Shi, X. S.; Bi, Y. C.; Yang, W.; Guo, X. D.; Jiang, Y.; Wan, C. J.; Li, L. Y.; Bai, Y. B.; Guo, J.; Wang, Y. J.; Chen, X. J.; Wu, B.; Sun, H. B.; Liu, W. L.; Wang, J. F.; Xu, C. Q., $Ca^{2+}$ regulates T-cell receptor activation by modulating the charge property of lipids. *Nature* **2013,** *493* (7430), 111-115.
4. Bakhti, M.; Snaidero, N.; Schneider, D.; Aggarwal, S.; Mobius, W.; Janshoff, A.; Eckhardt, M.; Nave, K. A.; Simons, M., Loss of electrostatic cell-surface repulsion mediates myelin membrane adhesion and compaction in the central nervous system. *Proc. Natl. Acad. Sci. U. S. A.* **2013,** *110* (8), 3143-3148.
5. Busscher, H. J.; van der Mei, H. C., How Do Bacteria Know They Are on a Surface and Regulate Their Response to an Adhering State? *PLoS Pathog.* **2012,** *8* (1), e1002440.

6. Dubiel, E. A.; Martin, Y.; Vermette, P., Bridging the Gap Between Physicochemistry and Interpretation Prevalent in Cell-Surface Interactions. *Chem. Rev.* **2011,** *111* (4), 2900-2936.

7. Kim, H. J.; Heo, C. H.; Kim, H. M., Benzimidazole-Based Ratiometric Two-Photon Fluorescent Probes for Acidic pH in Live Cells and Tissues. *J. Am. Chem. Soc.* **2013,** *135* (47), 17969-17977.

8. Haupt, A.; Campetelli, A.; Bonazzi, D.; Piel, M.; Chang, F.; Minc, N., Electrochemical Regulation of Budding Yeast Polarity. *PLoS. Biol.* **2014,** *12* (12), e1002029.

9. Wong, J. Y.; Langer, R.; Ingber, D. E., Electrically conducting polymers can noninvasively control the shape and growth of mammalian-cells. *Proc. Natl. Acad. Sci. U. S. A.* **1994,** *91* (8), 3201-3204.

10. Khitrin, A. K.; Khitrin, K. A.; Model, M. A., A model for membrane potential and intracellular ion distribution. *Chem. Phys. Lipids* **2014,** *184*, 76-81.

11. Wilson, W. W.; Wade, M. M.; Holman, S. C.; Champlin, F. R., Status of methods for assessing bacterial cell surface charge properties based on zeta potential measurements. *J. Microbiol. Methods* **2001,** *43* (3), 153-164.

12. Gross, D.; Loew, L. M.; Webb, W. W., Optical imaging of cell-membrane potential changes induced by applied electric-fields. *Biophys. J.* **1986,** *50* (2), 339-348.

13. Chen, B. D.; Le, W. J.; Wang, Y. L.; Li, Z. Q.; Wang, D.; Ren, L.; Lin, L.; Cui, S. B.; Hu, J. J.; Hu, Y. H.; Yang, P. Y.; Ewing, R. C.; Shi, D. L.; Cui, Z., Targeting Negative Surface Charges of Cancer Cells by Multifunctional Nanoprobes. *Theranostics* **2016,** *6* (11), 1887-1898.

14. Wang, W.; Foley, K.; Shan, X.; Wang, S. P.; Eaton, S.; Nagaraj, V. J.; Wiktor, P.; Patel, U.; Tao, N. J., Single cells and intracellular processes studied by a plasmonic-based electrochemical impedance microscopy. *Nat. Chem.* **2011,** *3* (3), 249-255.

15. Liu, X. W.; Yang, Y. Z.; Wang, W.; Wang, S. P.; Gao, M.; Wu, J.; Tao, N. J., Plasmonic-Based Electrochemical Impedance Imaging of Electrical Activities in Single Cells. *Angew. Chem.-Int. Edit.* **2017,** *56* (30), 8855-8859.

16. Takahashi, Y.; Shevchuk, A. I.; Novak, P.; Babakinejad, B.; Macpherson, J.; Unwin, P. R.; Shiku, H.; Gorelik, J.; Klenerman, D.; Korchev, Y. E.; Matsue, T., Topographical and electrochemical nanoscale imaging of living cells using voltage-switching mode scanning electrochemical microscopy. *Proc. Natl. Acad. Sci. U. S. A.* **2012,** *109* (29), 11540-11545.

17. Polcari, D.; Dauphin-Ducharme, P.; Mauzeroll, J., Scanning Electrochemical Microscopy: A Comprehensive Review of Experimental Parameters from 1989 to 2015. *Chem. Rev.* **2016,** *116* (22), 13234-13278.

18. Perry, D.; Nadappuram, B. P.; Momotenko, D.; Voyias, P. D.; Page, A.; Tripathi, G.; Frenguelli, B. G.; Unwin, P. R., Surface Charge Visualization at Viable Living Cells. *J. Am. Chem. Soc.* **2016,** *138* (9), 3152-3160.

19. Page, A.; Perry, D.; Young, P.; Mitchell, D.; Frenguell, B. G.; Unwin, P. R., Fast Nanoscale Surface Charge Mapping with Pulsed-Potential Scanning Ion Conductance Microscopy. *Anal. Chem.* **2016,** *88* (22), 10854-10859.

20. Wu, F.; Campos, I.; Zhang, D. W.; Krause, S., Biological imaging using light-addressable potentiometric sensors and scanning photo-induced impedance microscopy. *Proc. R. Soc. A-Math. Phys. Eng. Sci.* **2017,** *473* (2201), 1-20.

21. Das, A.; Chen, T.-C.; Yang, C.-M.; Lai, C.-S., A high-speed, flexible-scanning chemical imaging system using a light-addressable potentiometric sensor integrated with an analog micromirror. *Sensors*

*and Actuators B-Chemical* **2014,** *198*, 225-232.

22. Miyamoto, K.-i.; Itabashi, A.; Wagner, T.; Schoening, M. J.; Yoshinobu, T., High-speed chemical imaging inside a microfluidic channel. *Sensors and Actuators B-Chemical* **2014,** *194*, 521-527.

23. Zhang, D.-W.; Wu, F.; Wang, J.; Watkinson, M.; Krause, S., Image detection of yeast Saccharomyces cerevisiae by light-addressable potentiometric sensors (LAPS). *Electrochemistry Communications* **2016,** *72*, 41-45.

24. Cornell, R., Cell-substrate adhesion during cell culture: An ultrastructural study. *Experimental Cell Research* **1969,** *58* (2), 289-295.

25. Kreysing, E.; Hassani, H.; Hampe, N.; Offenhausser, A., Nanometer-Resolved Mapping of Cell-Substrate Distances of Contracting Cardiomyocytes Using Surface Plasmon Resonance Microscopy. *ACS Nano* **2018,** *12* (9), 8934-8942.

26. Zhang, D.-W.; Wu, F.; Krause, S., LAPS and SPIM Imaging Using ITO-Coated Glass as the Substrate Material. *Anal. Chem.* **2017,** *89* (15), 8129-8133.

27. Chen, L.; Zhou, Y.; Jiang, S.; Kunze, J.; Schmuki, P.; Krause, S., High resolution LAPS and SPIM. *Electrochemistry Communications* **2010,** *12* (6), 758-760.

28. Wang, J.; Zhou, Y.; Watkinson, M.; Gautrot, J.; Krause, S., High-sensitivity light-addressable potentiometric sensors using silicon on sapphire functionalized with self-assembled organic monolayers. *Sensors and Actuators B-Chemical* **2015,** *209*, 230-236.

29. Welden, R.; Scheja, S.; Schoning, M. J.; Wagner, P.; Wagner, T., Electrochemical Evaluation of Light-Addressable Electrodes Based on $TiO_2$ for the Integration in Lab-on-Chip Systems. *Phys. Status Solidi A-Appl. Mat.* **2018,** *215* (15), 201800150.

30. Seo, D.; Lim, S. Y.; Lee, J.; Yun, J.; Chung, T. D., Robust and High Spatial Resolution Light Addressable Electrochemistry Using Hematite (alpha-Fe2O3) Photoanodes. *ACS Appl. Mater. Interfaces* **2018,** *10* (39), 33662-33668.

31. Suzurikawa, J.; Nakao, M.; Jimbo, Y.; Kanzaki, R.; Takahashi, H., A light addressable electrode with a TiO2 nanocrystalline film for localized electrical stimulation of cultured neurons. *Sensors and Actuators B-Chemical* **2014,** *192*, 393-398.

32. Wagner, T.; Shigiahara, N.; Miyamoto, K.; Suzurikawa, J.; Finger, F.; Schoning, M. J.; Yoshinobu, T., Light-addressable potentiometric sensors and light-addressable electrodes as a combined sensor-and-manipulator microsystem with high flexibility. In *26th European Conference on Solid-State Transducers, Eurosensor 2012*, Walczak, R.; Dziuban, J., Eds. Elsevier Science Bv: Amsterdam, 2012; Vol. 47, pp 890-893.

33. Khalid, W.; El Helou, M.; Murboeck, T.; Yue, Z.; Montenegro, J.-M.; Schubert, K.; Goebel, G.; Lisdat, F.; Witte, G.; Parak, W. J., Immobilization of Quantum Dots via Conjugated Self-Assembled Monolayers and Their Application as a Light-Controlled Sensor for the Detection of Hydrogen Peroxide. *ACS Nano* **2011,** *5* (12), 9870-9876.

34. Riedel, M.; Holzel, S.; Hille, P.; Schormann, J.; Eickhoff, M.; Lisdat, F., InGaN/GaN nanowires as a new platform for photoelectrochemical sensors - detection of NADH. *Biosens. Bioelectron.* **2017,** *94*, 298-304.

35. Choudhury, M. H.; Ciampi, S.; Yang, Y.; Tavallaie, R.; Zhu, Y.; Zarei, L.; Goncales, V. R.; Gooding, J. J., Connecting electrodes with light: one wire, many electrodes. *Chemical Science* **2015,** *6* (12), 6769-6776.

36. Parker, S. G.; Yang, Y.; Ciampi, S.; Gupta, B.; Kimpton, K.; Mansfeld, F. M.; Kavallaris, M.; Gaus, K.; Gooding, J. J., A photoelectrochemical platform for the capture and release of rare single cells. *Nature Communications* **2018,** *9*, 2288.

37. Vogel, Y. B.; Goncales, V. R.; Gooding, J. J.; Ciampi, S., Electrochemical Microscopy Based on Spatial Light Modulators: A Projection System to Spatially Address Electrochemical Reactions at Semiconductors. *Journal Of the Electrochemical Society* **2018,** *165* (4), 3085-3092.

38. Zhang, D. W.; Papaioannou, N.; David, N. M.; Luo, H.; Gao, H.; Tanase, L. C.; Degousee, T.; Samori, P.; Sapelkin, A.; Fenwick, O.; Titirici, M. M.; Krause, S., Photoelectrochemical response of carbon dots (CDs) derived from chitosan and their use in electrochemical imaging. *Mater. Horizons* **2018,** *5* (3), 423-428.

39. Tu, Y.; Ahmad, N.; Briscoe, J.; Zhang, D.-W.; Krause, S., Light-Addressable Potentiometric Sensors using ZnO Nanorods as the Sensor Substrate for Bioanalytical Applications. *Anal. Chem.* **2018,** *90* (14), 8708-8715.

40. Kashi, M. B.; Silva, S. M.; Yang, Y.; Goncales, V. R.; Parker, S. G.; Barfidokht, A.; Ciampi, S.; Gooding, J. J., Light-activated electrochemistry without surface-bound redox species. *Electrochim. Acta* **2017,** *251*, 250-255.

41. Yang, Y.; Ciampi, S.; Zhu, Y.; Gooding, J. J., Light-Activated Electrochemistry for the Two-Dimensional Interrogation of Electroactive Regions on a Monolithic Surface with Dramatically Improved Spatial Resolution. *Journal of Physical Chemistry C* **2016,** *120* (24), 13032-13038.

42. Peter, L. M., Dynamic Aspects of Semiconductor Photoelectrochemistry. *Chem. Rev.* **1990,** *90* (5), 753-769.

43. Benoit, J.; Cormier, M.; Wepierre, J., Comparative Effects of 4 Surfactants on Growth, Contraction and Adhesion of Cultured Human-Fibroblasts. *Cell Biol. Toxicol.* **1988,** *4* (1), 111-122.

44. Nyholm, T.; Slotte, J. P., Comparison of Triton X-100 penetration into phosphatidylcholine and sphingomyelin mono- and bilayers. *Langmuir* **2001,** *17* (16), 4724-4730.

45. Koley, D.; Bard, A. J., Triton X-100 concentration effects on membrane permeability of a single HeLa cell by scanning electrochemical microscopy (SECM). *Proc. Natl. Acad. Sci. U. S. A.* **2010,** *107* (39), 16783-16787.

46. Morandat, S.; El Kirat, K., Membrane resistance to Triton X-100 explored by real-time atomic force microscopy. *Langmuir* **2006,** *22* (13), 5786-5791.

47. Jaeger, C. D.; Bard, A. J., Spin trapping and electron-spin resonance detection of radical intermediates in the photo-decomposition of water at $TiO_2$ particulate systems. *J. Phys. Chem.* **1979,** *83* (24), 3146-3152.

48. Tan, S. Y.; Perry, D.; Unwin, P. R., Double layer effects in voltammetric measurements with scanning electrochemical microscopy (SECM). *J. Electroanal. Chem.* **2018,** *819*, 240-250.

49. Zoski, C. G.; Liu, B.; Bard, A. J., Scanning electrochemical microscopy: Theory and characterization of electrodes of finite conical geometry. *Anal. Chem.* **2004,** *76* (13), 3646-3654.

50. Fromherz, P., Joining microelectronics and microionics: Nerve cells and brain tissue on semiconductor chips. *Solid-State Electronics* **2008,** *52* (9), 1364-1373.

**TOC**